Fluid Inclusions in carpholite – bearing metasediments and blueschists from NE Oman: Constraints on P-T evolution

Aley K. El-Shazly[1] and Virginia B. Sisson[2]

[1]Department of Geology, Geography and Physics, University of Tennessee, Martin, TN 38238
[2]Department of Earth Science, Rice University, Houston TX 77005-1892
e-mail address: aelshazly@utm.edu

Submitted to European Journal of Mineralogy, April 22, 2002.
Revised version submitted March 24, 2003.

Fluid Inclusions in carpholite – bearing metasediments and blueschists from NE Oman: Constraints on P-T evolution

Abstract

Thrust sheets of the upper plate of the Saih Hatat window, NE Oman contain metasediments formed under lawsonite albite facies conditions. Quartz and Fe-Mg carpholite in these metasediments contain several types of fluid inclusions; most are two-phase at room T with an aqueous NaCl – H_2O or NaCl – $MgCl_2$ – H_2O solution. Texturally early fluid inclusions display a wide range of final melting (Tm_f) and homogenization (T_h) temperatures. The lowest Tm_f and T_h values were recorded for moderately sized inclusions occurring in clusters. Some of the highest Tm_f and T_h values (> 320°C) are recorded for isolated inclusions in Fe-Mg carpholite and quartz. In the lower plate epidote-blueschist facies metasediments, many fluid inclusions in quartz are decrepitated, with most of the surviving inclusions being 3 – phase, CO_2 – bearing, filled with a low salinity fluid with $XCO_2 < 0.05$. For all samples from both plates, isochores calculated for the few texturally early inclusions with low T_h values are consistent with their respective P-T estimates.

We conclude that inclusions with high T_h experienced post-entrapment stretching ± loss of H_2O during exhumation. Larger inclusions and inclusions in Fe-Mg carpholite were more strongly affected by these changes. Small isolated inclusions in relatively unstrained quartz have escaped these modifications and are useful for constraining peak conditions.

Key words: fluid inclusions, microthermometry, carpholite, high P metamorphism.

Abbreviations

Ab: albite, Act: actinolite, Alln: allanite; Ap: apatite, Cc: calcite, Chl: chlorite, Car: Fe-Mg carpholite, Crs: crossite, Czo: clinozoisite, Ctd: chloritoid, Dap: daphnite (Fe-chlorite), Ep: epidote, Fcar: Fe-carpholite, Fctd: Fe-chloritoid, Fgln: ferroglaucophane, Gln: glaucophane, Hm: hematite, Ill: illite, Jd: jadeite, Kln: kaolinite, Ky: kyanite, Mcar: Mg-carpholite, Musc: muscovite, Opq: opaque phase; Oxychl: oxychlorite; Pg: paragonite, Ph: phengite, Prl: pyrophyllite, Qz: quartz, Rt: rutile, S.F.: shape factor, Sud: sudoite, Tm: tourmaline, T_h: homogenization temperature, Tm_f: final melting temperature, Ttn: titanite, VESR: volume equivalent spherical radius, WM: white mica; Zrn: zircon.

1. Introduction

A study of fluid inclusions in metamorphic minerals provides a plethora of valuable information. To begin with, these inclusions may preserve fluids pre-dating or attending peak metamorphism. Microthermometric studies of inclusions trapped early and subsequently unmodified may help provide some constraints on pre-peak or peak metamorphic conditions (e.g. Andersen et al., 1989; Vry & Brown, 1991; Klemd et al., 1992; Hurai et al., 2000; Gao & Klemd, 2001). On the other hand, post-entrapment modification of the volume and shape of fluid inclusions in response to deformation, cooling or decompression can help constrain the retrograde P-T paths of their host rocks and hence provide some insight into the mechanism of their exhumation (e.g. Scambelluri, 1992; Winslow et al., 1994, Vallis & Scambelluri, 1996; Kuster & Stockhert, 1997; El-Shazly and Sisson, 1999; Bakker & Mamtani, 2000). In all cases, careful analysis of the fluid inclusion textures and microthermometric results holds the key to successful data interpretation (e.g. Bodnar et al., 1989; Sterner & Bodnar, 1989;

Vityk et al., 1994; 1995; Barker, 1995; Sterner et al., 1995; Vityk & Bodnar, 1995; Van den Kerkhof & Hein, 2001).

Fe-Mg carpholite and crossite are important index minerals characteristic of high pressure and relatively low temperature (high P/T) conditions. Nevertheless, their P-T stability fields are poorly constrained, mainly due to the paucity of experimental reversals and therefore reliable thermodynamic data and solution models for these two minerals. Accordingly, the P-T conditions of formation of Fe-Mg - carpholite bearing metasediments and crossite schists for several high P/T terranes (e.g. Calabria, Crete, Greece, New Caledonia, and Oman) are poorly constrained and controversial. One of these controversies applies to the high P/T rocks of Saih Hatat, Oman, where peak pressure estimates for Fe-Mg carpholite bearing metasediments by different authors differ by as much as 3 kbar, and where there is a strong disagreement over the shapes of the P-T paths of these rocks (cf. Goffé et al., 1988; El-Shazly, 1994, 1995, 1996; Vidal & Theye, 1996). In this paper, we present microthermometric data for fluid inclusions in Fe-Mg carpholite and quartz from the metasediments and prasinitic schists of NE Oman. The aim of this study is to provide additional constraints on the P-T evolution of these rocks, and a better understanding of the conditions of fluid entrapment.

2. Geological Setting

The Saih Hatat area in NE Oman is a domal window that exposes basement, shelf and foreland basin units structurally underlying the allochthonous Semail ophiolite, Haybi Complex and Hawasina basin units (Glennie et al., 1974; Fig. 1). The basement consists of Proterozoic quartz mica schists, metagreywackes and metabasites of the Hatat Formation, and recrystallized dolomites of the Hijam Formation, unconformably overlain by Ordovician quartzites and metasiltstones of the Amdeh Formation (Glennie et al. 1974; Le Métour et al., 1986). The overlying Permian to Cretaceous shelf units are predominantly metacarbonates with interbedded mafic, arenaceous and pelitic schists. Metamorphosed sandstones, conglomerates and a mélange overlie the shelf units either unconformably or tectonically, and are interpreted as the metamorphic equivalent of the Late Cretaceous Muti Formation (Le Métour et al., 1986; Robertson, 1987).

El-Shazly & Coleman (1990) subdivided the Saih Hatat area into three thrust-bounded regions (Fig. 1). Region I, consists of a tectonic mélange metamorphosed under lawsonite - albite facies conditions (El-Shazly, 1994), as well as an overthrust sheet of unmetamorphosed cherts, serpentinites and basalts (Hawasina Complex). Region II, consists of several thrust sheets of folded basement and shelf units, metamorphosed under lawsonite – albite to epidote – blueschist facies conditions. The structurally lowest Region III is predominated by calcareous mica schists and metacarbonates containing layers and lenses of mafic schists, metapelites, and quartz mica schists, all of which are considered part of the Permian Saiq Formation (Le Métour et al., 1986). These units exhibit an eastward increase in metamorphic grade from epidote - blueschist facies conditions in central Saih Hatat (zone A of El-Shazly et al., 1990) to eclogite facies conditions along the eastern coast near As-Sifah (zone C, Fig. 1). Miller et al. (1998) and Gregory et al. (1998) considered the boundary between Regions II & III as a major ductile discontinuity separating two plates with different structural and metamorphic features. Their upper plate, which includes imbricated unmetamorphosed to weakly metamorphosed units, corresponds to Regions I & II of El-Shazly & Coleman (1990), whereas the lower plate corresponds to Region III (Fig. 1).

3. P-T conditions of Metamorphism

Goffé et al. (1988) estimated the P-T conditions of metamorphism of the tectonic mélange of Region I at $T < 280°C$, $P > 8$ kbar. According to these authors, the structurally lower units of Region II were metamorphosed under lower P conditions of only 5 – 8 kbar at T of 250 – 380°C, hence displaying "local inverted metamorphic gradients" within the upper plate. Goffé et al. (1988) also concluded that all these rocks are characterized by "anticlockwise" P-T paths with peak temperatures reached before peak pressures. On the other hand, El-Shazly (1994; 1995; 1996) suggested that all mafic and pelitic rocks of Regions I and II were characterized by clockwise P-T paths, and that peak metamorphic conditions ranged from < 300°C, 3 – 6 kbar for the tectonic mélange to 380 – 430°C, 6.5 – 9 kbar for the structurally deepest units in Region II. For Region III, El-Shazly et al. (1990) and El-Shazly (2001) estimated their peak P-T conditions of metamorphism between 410 – 460°C, 6.5 – 8.5 kbar for zone A to 550 – 580°C, 12 – 16 kbar for zone C (see also Le Métour et al., 1990; Searle et al., 1994). According to El-Shazly (1994, 1995, 1996 & 2001; Fig. 1), there is a systematic down-section increase in metamorphic grade within Saih Hatat, with no evidence of inverted metamorphic gradients.

In this study, we present fluid inclusion data for (i) three Fe-Mg carpholite – bearing samples collected from different structural and/or stratigraphic levels in Regions I and II, and (ii) three samples collected from zone A of Region III. Fluid inclusion data for the higher grade eclogites of zone C, Region III were presented in El-Shazly and Sisson (1999). These data provide important constraints on the P-T paths and tectonic evolution of the high P/T rocks of Saih Hatat.

4. Fluid Inclusion Data

4.1 Petrography of the studied samples

Mineral assemblages and key petrographic features of the six samples studied here are listed in Table 1. Sample R-97 is a carpholite - bearing boudinaged quartz – calcite vein within the carpholite - bearing schists of Hamiriya, south of Ruwi (Fig. 1). These schists are part of the matrix of a metamorphosed tectonic mélange that contains blocks of marble and metabasites as well as lenses of lawsonite chlorite schists and phyllites (El-Shazly, 1994). The vein is of the stretched crystal fiber type (Ramsay & Huber, 1983), consisting primarily of elongated to fibrous quartz, calcite and Fe-Mg carpholite, growing perpendicular to the vein walls. Fe-Mg carpholite (X_{Fe} = 0.63 - 0.69) is prismatic to fibrous and is crosscut by veinlets of calcite. The quartz crystals have serrate edges and are elongated parallel to the carpholite fibers. Deformation caused strong undulatory extinction or complete recrystallization to finer–grained, strain - free polygonal crystals. All subgrain boundaries in the strained quartz crystals are oriented at a high angle to the original serrate grain boundaries, and are decorated by trails of secondary fluid inclusions. Boundaries of the strain - free quartz crystals are all decorated by decrepitated wispy fluid inclusions.

Sample Mj-14 is a metamorphosed paleosol in the Saiq formation (Goffé et al., 1988; Region II; Fig. 1; Table 1). Most of the quartz grains in this sample have retained their detrital angular shapes, with some (~ 10%) showing undulose extinction. Clusters of finer-grained polygonal quartz crystals are interpreted as clasts of chert.

Sample Am-4 (Region II, Fig. 1) is a strongly lineated carpholite - quartz schist (Table 1). It is crosscut by several veinlets of the stretched fiber type (Ramsay and Hubert, 1983), the largest of which is 2.5 cm thick and contains quartz + Fe-Mg carpholite + chlorite + calcite. Fe-Mg carpholite occurs as fibrous to prismatic medium grained crystals that define a foliation (S_2) and lineation, although a few crystals are oriented parallel to the folded foliation (S_1). Vein carpholite is identical in composition to that of the host rock. Most quartz is strain - free and polygonized. Vein quartz is stretched parallel to S_2 and perpendicular to the vein wall, and has serrate edges and strong undulose extinction. Most subgrain boundaries in quartz are oriented at a high angle to the stretching direction (S_2). Fine - grained polygonized quartz occurs along some of the serrate grain boundaries. Minor amounts of chlorite replace carpholite along rims and fractures.

Samples III-90, III-176 and III-181 were all collected from the Saiq units of the lower plate (zone A, Region III; Fig. 1; Table 1). All three samples are characterized by strong S-C fabrics or folded foliations. Their quartz is fine-grained (~ 0.1 mm), polygonized, and mostly (> 80%) strain free. Only a few coarser grained quartz crystals show some undulose extinction.

4.2 Fluid Inclusion Petrography

In the samples studied, fluid inclusions occur in quartz and Fe-Mg carpholite. We classified these inclusions according to the number and type of fluid phases observed at room T, their host minerals, and their textures into:

1- A_{Qz}: Isolated, two-phase (liquid + vapor; L + V) inclusions in quartz.
2- B_{Qz}: Clusters of two-phase inclusions in quartz that do not cross grain boundaries, and are independent of subgrain boundaries.
3- C_{Qz}: Trails of two - phase inclusions in quartz that (in most samples) cross grain boundaries.
4- X_{Qz}: Three - phase (CO_2 - bearing) fluid inclusions in quartz that are either solitary or occur in clusters.
5- A_{Car}: Isolated, two-phase inclusions in Fe-Mg carpholite.
6- C_{Car}: Two - phase inclusions in Fe-Mg carpholite that occur in trails that cross grain boundaries.

In addition to these types, wispy to highly irregular, decrepitated inclusions decorate the quartz grain boundaries in most samples. Trails of monophase inclusions crossing grain boundaires are also common in some samples (e.g. Mj-14). Because these two types are not amenable to microthermometric measurements, they are not further discussed.

4.2.1 Upper Plate samples:

R-97 has types A_{Car}, A_{Qz}, B_{Qz} and C_{Qz}. Type A_{Car} inclusions are small (3-10 μm), and either tubular or slightly elongated parallel to the c-axis of their host carpholite crystals (Figs. 2a & b). Almost all inclusions are characterized by the same degree of fill (~ 5% vapor). Types A_{Qz} and B_{Qz} inclusions have various shapes and sizes, but a uniform degree of fill (5% vapor). The largest inclusions of these two types are highly irregular (i.e. have the lowest shape factors of ~ 3; cf. Bodnar et al., 1989), but are generally unrelated to subgrain boundaries or other deformational features in the host quartz. Types C_{Qz} and C_{Car} occur along the same healed fractures that cross grain boundaries at high angles (~ 80°) to the carpholite c- axis (Fig. 2d). Inclusions of these two types often have different sizes and degrees of fill (even when they occur along the same healed fracture), with a few showing some evidence of necking down. Overall, C_{Qz} and C_{Car} inclusions are smaller with lower shape factors (~ 6 – 7) compared to types A and B inclusions.

Fluid inclusions in Mj-14 are of types A_{Qz}, B_{Qz} and C_{Qz}. These inclusions are characterized by many different shapes, sizes and degrees of fill, and are more common in the large, angular (detrital) quartz crystals. Types A_{Qz} and B_{Qz} are fairly large (4 - 14 μm) and equant (shape factors of 8 - 10), but with variable degrees of fill (5 - 10% vapor). Type C_{Qz} inclusions are smaller and more irregular than types A_{Qz} and B_{Qz}, and define at least three sets of healed fractures (C_1 – C_3; arranged from oldest to youngest through crosscutting relations), none of which cross grain boundaries. C_1 runs parallel to the few subgrain boundaries in its host quartz.

In Am-4, polygonized quartz crystals contain inclusions of types A, B and C that are small (3- 5 μm) with high shape factors (7- 10), and variable degrees of fill. Type C_{Qz} inclusions define healed fractures across grain boundaries oriented at a high angle to the elongation of their host crystals (and carpholite fibers). As in samples R-97 and Mj-14, these healed fractures run parallel to the subgrain boundaries and are more common within the stretched fiber veinlets.

4.2.2. Lower Plate Samples:

Samples III-181 and III-176 are characterized by very few fluid inclusions of types A_{Qz} & B_{Qz}. Most of these inclusions are small (~ 5 μm) with a variety of shapes (but mostly low shape factors of 3 - 5) and variable degrees of fill (1 - 10% vapor). Many of these inclusions show evidence of necking down. In both samples, fluid inclusions on healed fractures are monophase, whereas all grain boundaries are decorated with decrepitated inclusions. In sample III-90, most inclusions are isolated, highly irregular (S.F. = 2 - 5; Fig. 2e), and CO_2 - bearing. These type X_{Qz} inclusions range in size from 10 - 35 μm, and are characterized by 10% vapor and 1 - 5% CO_2.

4.3 Microthermometry

4.3.1 Analytical Techniques

Fluid inclusions in Fe-Mg carpholite and quartz were analyzed on a Fluid Inc. USGS - type gas flow heating/freezing stage at Rice University. The stage was calibrated using synthetic fluid inclusions (Bodnar et al., 1989) at -56.6, 0, 10.2, and 374°C. All measurements reported in this paper were done with increasing temperature at rates of 0.5°C and 1 – 5°C/ minute for melting and homogenization, respectively. Initial melting temperatures (Tm_e) were recorded for many but not all inclusions. Temperatures of final melting of ice (Tm_f) and homogenization (T_h) were replicated; precision is ± 0.2°C for Tm_f and ± 2°C for T_h. Tm_f and T_h were almost always determined for the same inclusion, where the freezing experiment was followed by heating to determine T_h. Fluid salinities (expressed as weight % NaCl equivalent) and densities were calculated with the equations of state of Zhang and Frantz (1987) and Brown and Lamb (1989) for the NaCl – H_2O and the H_2O - NaCl - CO_2 systems, respectively, using program FLINCOR

(Brown, 1989). The extrapolated isochores have error bars of ~ 1 kbar. For type X_{Qz}, XCO_2 was determined from the homogenization T of the carbonic fluid and the volume fraction of CO_2 at room T. The results are summarized in Table 2.

4.3.2 Microthermometric Results

4.3.2.1 Upper Plate samples:

Tm_e for type A_{Car} inclusions in R-97 range from –28 to –31°C. Most of type A_{Qz} and B_{Qz} inclusions R-97 yield Tm_e values in the same range, with only ~ 25% of these two types recording lower Tm_e of –75 to –37°C. Tm_f for all types of inclusions range from –3.8 to +1.8°C, with most values clustering between –1.5 and 0°C (Fig. 3a). Fluids trapped in type A_{Car} inclusions appear to be slightly more saline (Tm_f = -0.5 to –2) than those in types A_{Qz} and B_{Qz}, whereas type C_{Qz} inclusions appear to be more aqueous (Fig. 3a).

All inclusions in R-97 homogenize by the disappearance of the vapor phase ($V \rightarrow L$). Homogenization temperatures range from 117.7°C to > 310°C, with about 60% of all measurements for types A_{Qz} and B_{Qz} falling between 130 and 170°C (Fig. 4a). Although fluid inclusions in carpholite show some scatter in T_h values, almost all tubular or elongated type A_{Car} inclusions are characterized by T_h > 310°C (Fig. 4a). Most of the "secondary" fluid inclusions in trails that cross grain boundaries (types C_{Car} and C_{Qz}) homogenize between 160 and 170°C.

Plots of T_h versus the volume equivalent spherical radius (VESR) of Hall & Sterner (1993) and the shape factor (Bodnar et al., 1989) for fluid inclusions from R-97 show that types A_{Car} and C_{Car} inclusions that record some of the highest T_h values have relatively high shape factors (i.e. are closest in shape to negative crystals) and small sizes (Figs. 5a and b). Figure 5a also shows a weak inverse correlation between T_h and size for types

A_{Qz} and A_{Car}. Figure 5b shows that for types A_{Car} and A_{Qz}, inclusions with high T_h values are characterized by relatively high shape factors whereas the lowest T_h (117.7°C) is recorded for a highly irregular inclusion with the lowest shape factor. On the other hand, most type B_{Qz} inclusions are characterized by relatively high shape factors and low T_h.

A plot of T_h versus Tm_f shows that most inclusions cluster at values of –1.6 to 0°C and 130 – 170°C (Fig. 5c). A weak negative correlation is displayed by types A_{Car} (and A_{Qz}?), whereas almost all type B_{Qz} inclusions display a narrow range of relatively low T_h values. Most inclusions with T_h > 250°C are characterized by lower degrees of fill (volume % vapor ~ 10 - 20).

In Mj-14, most fluid inclusions are characterized by Tm_e between –21 and –34°C, with ~ 15% of inclusions studied recording values between –42 and –48°C. Final ice melting temperatures for most type A inclusions ranged between –1 and 0°C, whereas for type B inclusions Tm_f values were bimodal at –0.5 to 0 and –8.5 to –7.5°C (Fig. 3b). Most type B inclusions with low Tm_f values are also characterized by Tm_e between –42 and –48°C. On the other hand, type C inclusions show considerable scatter in Tm_f values, but overall are characterized by lower salinities compared to types A and B inclusions, particularly for types C_2 and C_3.

Homogenization temperatures (V→L) for types A and B inclusions cluster between 100 and 130°C, and 120 to 150°C for type C inclusions (Fig. 4b). Very few inclusions are characterized by T_h > 320°C. Type A inclusions with T_h > 170°C are characterized by intermediate sizes (Fig. 6a) and relatively high shape factors (Fig. 6b). Although all type B inclusions within the same cluster have the same T_h, their Tm_f values vary (Fig. 6a).

Most fluid inclusions in sample Am-4 show initial melting temperatures between –21 and –31°C, with ~ 25% of inclusions studied recording Tm_e between –38 and –48°C and one recording a value of –74°C. Final melting temperatures for all such inclusions range from –7.8 to 0°C, but cluster between –4.8 and –5.5°C (Fig. 3c). Homogenization temperatures for these inclusions (V→L) range from 143 to > 340°C, but cluster between 200 and 240°C (Fig. 4c). Inclusions with T_h < 150°C are relatively small (Fig. 7a) and approach negative crystal shapes (Fig. 7b). Most inclusions with T_h > 220°C are also characterized by negative crystal shapes and low degrees of fill (Figs. 7b & c).

4.3.2.2 Lower plate samples:

Microthermometric measurements on the few fluid inclusions preserved in zone A samples show a large scatter in Tm_e, Tm_f and T_h values. Initial melting temperatures for most inclusions in sample III-181 range from –44 to –46°C (Table 2). On the other hand, most inclusions in III-90 and III-176 contain three-phases with Tm_e between –57 and –53°C, and display a second jerk of the bubble between –22 and –21°C. Clathrate melting was difficult to observe, but a few temperatures were recorded between 9.2 to 11.9°C. Final ice melting temperatures show a wide scatter between –9 and 0°C, but cluster between –1 and 0°C (Fig. 8a). With the exception of a unique inclusion in III-176, all inclusions homogenize by the disappearance of the vapor (V→L) at T between 95 and 306°C, with a mode at 220 – 280°C. Most inclusions from sample III-181 homogenize at T > 310°C. For the CO_2-bearing inclusions, homogenization of the CO_2 - saline solution phases took place at T of 29 - 31°C. Tm_f and T_h are not clearly correlated for these samples, although elimination of data points with Tmf > 0°C produces a very weak negative correlation (Fig. 9).

5. Data Interpretation

Each of the upper plate samples R-97, Mj-14 and Am-4 is considered to have experienced unique P-T conditions and paths (e.g. El-Shazly, 1995; 1996) because they were not collected from the same thrust sheet or unit. These samples have therefore probably interacted with and trapped different fluids at different P-T conditions, and their microthermometric data are best interpreted individually. On the other hand, data for samples III-90, III-176, and III-181 will be considered collectively as they were collected from the same metamorphic zone in the lower plate. Nevertheless, all samples have some common textural and microthermometric features that we discuss collectively before delving into a detailed discussion for each sample.

5.1 Inclusion textures:

In all samples studied, types A and B inclusions are texturally early and appear to have formed during the crystallization of their host quartz and carpholite. Among these types, A_{Car} inclusions are of particular interest, since they may enclose fluid trapped during prograde metamorphism (close to or at peak pressure). Inclusions of types A_{Qz} and B_{Qz} may have also preserved the same fluid provided that their host quartz did not recrystallize during exhumation. On the other hand, type C inclusions developed at a later stage by the brittle failure of their host crystals, with those defining trails that cross grain boundaries clearly being “secondary”. Lower plate samples (all of which show evidence of several deformational/ folding events) are characterized by the paucity of pristine, texturally early (types A and B) fluid inclusions, and the abundance of decrepitated ones.

5.2 Eutectic melting and fluid compositions:

In most upper plate samples, Tm_e values indicate that types A & B inclusions are filled with a low salinity (mostly < 12 wt. % NaCl equivalent) aqueous fluid belonging to the system NaCl – H_2O, although some inclusions contain a more saline fluid or some divalent cations (Goldstein & Reynolds, 1994). Type C inclusions are also filled with aqueous NaCl – H_2O solutions, but are generally less saline than those of types A and B. In Mj-14 with more than one generation of type C inclusions, the younger the inclusion trails are, the lower the salinity of their enclosed fluid becomes, as indicated by their higher Tm_f values (Fig. 3b). The large scatter in Tm_f values recorded for inclusions in Mj-14 suggests that they are filled with at least two different types of fluids; a low salinity aqueous NaCl – H_2O solution, and a slightly more saline fluid containing $MgCl_2$ and/or $CaCl_2$ (Goldstein & Reynolds, 1994; Table 2; Fig. 3b). Entrapment of different fluids in quartz in Mj-14 is not surprising given (i) the detrital nature of these quartz grains which were derived from different rock types, (ii) that these crystals have largely escaped recrystallization during subsequent high P/T metamorphism, and (iii) that there are multiple generations of fractures that formed at different stages of evolution of this rock. The preponderance of CO_2 - bearing inclusions in lower plate mafic and arenaceous schists (e.g. III-90) can be explained by the proximity of these samples to the contact between these schists and the enclosing calcareous rocks (Fig. 1).

5.3 Final melting and homogenization temperatures:

Whereas a scatter in Tm_e values is interpreted to indicate entrapment of different fluids during crystallization of their host minerals (e.g. Mj-14), interpreting the scatter in Tm_f

and T_h values observed for the same sample is not as straightforward. A scatter in Tm_f values could result from entrapment of different fluids with different salinities, and/or from post-entrapment modification of the fluid composition through leakage and preferential loss of H_2O (e.g. Hall & Sterner, 1993; Bakker & Jansen, 1991;1994; Cordier et al., 1994; Audétat & Gunther, 1999). Similarly, the scatter in T_h values could be the result of either entrapment of one or more fluids with different densities, possibly during the different stages of crystal growth/ recrystallization, or post-entrapment re-equilibration of some fluid inclusions as their host rock experienced different P-T conditions during its various stages of evolution (e.g. Bodnar et al., 1989; Barker, 1995; Vityk & Bodnar, 1995a; Küster & Stöckhert, 1997).

Attributing the scatter in Tm_f and T_h values recorded for each of the Saih Hatat samples to entrapment of different fluids would require a relationship between the fluid inclusion assemblage, Tm_f , and T_h values, such as clustering of data points into clear groups (bi- or tri-modal distribution on histograms). However, such a relationship exists only for sample Mj-14 (Fig. 3b; Table 2), which is interpreted to have trapped different fluids. For all other samples, the scatter in T_h (and to a lesser extent Tm_f; Figs. 3 & 4) is attributed to post-entrapment modification of these inclusions.

Post-entrapment modification of fluid inclusions in metamorphic minerals is fairly common during exhumation (Barker, 1995; Vityk & Bodnar, 1995a; Barker & Mamtani, 2000), and is recorded for several high P/T metamorphic rocks (e.g. Touret, 1992; Vallis & Scambelluri, 1996; Küster & Stöckhert, 1997; Scambelluri et al., 1998; El-Shazly, &

Sission, 1999), where it is largely attributed to an increase in the internal pressure of the inclusion (e.g. Sterner & Bodnar, 1989). Post-entrapment modification includes:

1- Necking down, which produces two or more daughter inclusions with variable shapes, sizes, and V:L ratios (e.g. Roedder, 1984)
2- Stretching of the inclusion, hence increasing its volume and therefore T_h (e.g. Bodnar et al., 1989; Vityk & Bodnar, 1995b)
3- Leakage of the liquid from the inclusion, often resulting in preferential loss of H_2O, in turn manifested by a decrease in Tm_f and an increase in V:L ratios (e.g. Hall & Sterner, 1993; Sterner et al., 1995; Audétat & Gunther, 1999).

Not all fluid inclusions are equally affected by these changes. Larger inclusions are generally considered more susceptible to post-entrapment changes during exhumation (e.g. Bodnar et al., 1989).

Whereas necking down can be detected by careful textural observations, leakage and particularly stretching are more difficult to identify. For this purpose, plots of Tm_f versus T_h coupled with careful documentation of inclusion size, shape, and V:L ratios are useful. Stretching of an inclusion would increase T_h without changing Tm_f along a vertical trajectory on $T_{mf} – T_h$ plots. On the other hand, stretching accompanied by water loss would increase T_h and decrease T_{mf}, possibly producing an array of data points that define a negative trend on $T_{mf} – T_h$ plots, whereas stretching coupled with addition of water to the inclusion would increase both T_h and Tm_f, producing an array of points with a positive trend. For sample R-97, the scatter and weak negative trend on a Tm_f - T_h plot displayed by fluid inclusions in carpholite (types A_{Car} & C_{Car}, Fig. 5c) suggests that some of these inclusions underwent stretching and preferential loss of H_2O. This conclusion is supported by the moderate to high shape factors (arising from their tubular shapes; Figs. 2a & b; 5b) of most inclusions with $T_h > 300°C$. Post-entrapment reequilibration resulting from increased internal pressure is often accompanied by an increase in shape factors (Bodnar et al., 1989). The same $Tm_f – T_h$ plot shows that data points for types A_{Qz} and B_{Qz} are much less scattered particularly for Tm_f. Eliminating all points with $Tm_f > 0°C$, the scatter for type A_{Qz} inclusions defines a short vertical trajectory, suggesting that the inclusions in Qz underwent some stretching with little or no loss of water. We therefore conclude that the original fluid trapped in type A_{Car}, A_{Qz} and B_{Qz} inclusions was a low salinity aqueous solution (T_h ~ 130-160°C; Tm_f: -1.5-0°C). Whereas type A_{Car} inclusions stretched and leaked to various degrees during exhumation, types A_{Qz} and B_{Qz} were mostly unaffected by this process, with only a few inclusions undergoing some stretching and displaying $T_h \approx 250°C$ (Fig. 5a).

Tm_f - T_h plots for sample Mj-14 show a much wider scatter. Nevertheless, Tm_f values cluster in two distinct groups; (-6 & –12; and –3 & 0°C with $T_h < 160°C$ for both groups) suggesting the entrapment of more than one type of fluid as pointed out earlier. Because most of the inclusions that homogenize at T > 160°C are characterized by relatively high V:L ratios, moderate sizes (7-10 μm) and high shape factors (> 6; Figs. 6a & b), we conclude that these inclusions have also re-equilibrated by stretching ± leakage.

For sample Am-4, Tm_f and T_h values display a near vertical trajectory on the Tm_f - T_h plot (Fig. 7c). Given that the earliest inclusions (type A_{Qz}) are characterized by T_h of 140

- 220°C, whereas most inclusions with higher T_h values have low degrees of fill, relatively small sizes, and intermediate to high shape factors (Fig. 7a & b), we conclude that the latter group underwent stretching ± leakage.

For the lower plate samples, the Tm_f - T_h plot does not show a clear pattern (Fig. 9). Nevertheless, almost all aqueous (CO_2 – free) inclusions with T_h values between 96 and 250°C are texturally early with high degrees of fill (~ 5 volume % vapor), whereas many inclusions with T_h > 250°C have a high shape factor. This suggests that many inclusions experienced significant stretching and leakage during exhumation. This would explain the observed scatter in Tm_f & T_h and is consistent with the abundance of decrepitated inclusions along grain boundaries. It therefore seems that inclusion survival depended primarily on its location relative to migrating grain boundaries, rather than inclusion size or shape.

5.4 Isochores and Conditions of Fluid Entrapment

Post-entrapment modification of several fluid inclusions in the studied samples means that isochores calculated for these inclusions are not representative of conditions of their entrapment because the assumption of constant volume after entrapment no longer holds. To obtain meaningful isochores that would help constrain the P-T conditions of crystallization of the host minerals requires careful selection of microthermometric data. We have therefore calculated isochores only for inclusions that appear primary (types A and B), have the lowest T_h values, the highest degrees of fill ($\leq$5 volume % vapor), intermediate to high shape factors, and average sizes (~ 4 – 8 μm). The rationale behind these criteria is that small inclusions with negative crystal shapes and high salinities often represent the final product of post entrapment modification and/or preferential water loss (Bodnar et al., 1989; Hall & Sterner, 1993), whereas large inclusions with a large number of reentrants (low shape factors) are considered more susceptible to stretching and leakage (e.g. Bodnar et al, 1989).

For sample R-97, all isochores calculated for type A_{Car} inclusions that satisfy the above listed criteria plot outside all P-T estimates for the metamorphism of the upper plate mélange (Goffé et al., 1988; El-Shazly, 1994; 1995; 1996; Fig. 10). On the other hand, a few isochores of type A_{Qz} inclusions satisfying the same selection criteria straddle El-Shazly's (1995; 1996) lower P limit for these rocks. This suggests that whereas all inclusions in carpholite underwent significant stretching and/ or leakage during exhumation, inclusions in quartz were less affected by these processes.

For Mj-14, isochores for inclusions of types A_{Qz} and B_{Qz} that satisfy the above criteria are consistent with the P-T estimates of El-Shazly (1996), but define pressures significantly lower than the estimates of Goffé et al. (1988). Nevertheless, these results may be fortuitous as some or all of these inclusions may have formed during a pre-Permian igneous or metamorphic event that crystallized the host quartz. These inclusions may have thus survived the Cretaceous high P/T metamorphic event unmodified as their host quartz is relatively undeformed.

Isochores calculated for type A_{Qz} inclusions in Am-4 that satisfy the above listed criteria are also consistent with the P-T estimates of El-Shazly (1995; 1996) for the schists of the Saiq and Hatat formations of this plate (Fig. 10). It should be noted that calculation of an activity corrected petrogenetic grid for Am-4 that assumes that Car, Prl and Qz are all in equilibrium with Chl yields P-T estimates inconsistent with the calculated isochores. These estimates are also higher in P and lower in T than P-T estimates for overlying and underlying units from the same area (El-Shazly, 1995; 1996). This leads us to conclude that Chl (formed along fractures and rims of Car), never equilibrated with Car and Prl.

For the lower plate samples, isochores calculated for CO_2 – bearing inclusions as well as for the few aqueous inclusions that satisfy our selection criteria, are consistent with the P-T estimates for these rocks (El-Shazly, 2001). The intersection of isochores for both types of inclusions at ~ 420°C, 7 kbar (Fig. 11) suggests that these rare inclusions were hardly affected by post-entrapment processes during the exhumation of the lower plate units. Although this consistency does not prove that the P-T estimates of El-Shazly (1995; 1996; 2001) are correct, it lends credence to them and to the criteria established for the selection of inclusions for meaningful isochore calculations.

6. Conclusions

1- Fluid inclusions in Car and Qz underwent stretching ± H_2O loss during exhumation. Only texturally early, moderately sized (5 – 10 μm) inclusions with a high degree of fill, intermediate shape factors, and relatively low T_h values may preserve fluids representative of the conditions of entrapment, and are therefore suitable for meaningful isochore calculations.

2- Inclusions in Fe-Mg carpholite were more susceptible to post-entrapment modifications than intermediate to small inclusions in Qz (types A_{Qz} & B_{Qz}).

3- Only a few inclusions in lower plate samples survived the two or more deformational events; most inclusions either decrepitated, leaked, necked down, or stretched.

4- Isochores for primary inclusions interpreted to have escaped post-entrapment modification during exhumation are consistent with El-Shazly's (1995; 1996; 2001) P-T estimates and P-T paths for their host samples. On the other hand, the higher P estimates of Goffé et al. (1988) would require these inclusions to withstand internal pressures > 3 kbar, which is inconsistent with the experimental results of Bodnar et al. (1989) on the decrepitation of similar sized inclusions in quartz.

Acknowledgements

AES thanks the Omani Ministry of Commerce and Industry for logistical support with field work in Oman, and Dr. J. Rogers for help with drafting figure 1. The authors thank Prof. T. Andersen and an anonymous reviewer for comments that improved the manuscript substantially.

References

Andersen, T., Burke, E.A.J., Austrheim, H., (1989): Nitrogen - bearing aqueous fluid inclusions in some eclogites from Western Gneiss Region of the Norwegian Caledonides. Contributions to Mineralogy and Petrology, **103**, 153 - 165.

Audétat, A. & Gunther, D. (1999): Mobility and H_2O loss from fluid inclusions in natural quartz crystals. *Contributions to Mineralogy and Petrology*, **137**, 1-14.

Bakker, R.J. & Jansen, B.H. (1991). Experimental post-entrapment water loss from synthetic fluid inclusions in natural quartz. *Geochimica et Cosmochimica Acta*, **55**, 2215 – 2230.

Bakker, R.J. & Jansen, B.H. (1994). A mechanism for preferential H_2O leakage from fluid inclusions in quartz, based on TEM observations. *Contributions to Mineralogy and Petrology*, **116**, 7 – 20.

Bakker, R.J. & Mamtani, M.A. (2000): Fluid inclusions as metamorphic process indicators in the Southern Aravalli Mountain belt, India. *Contributions to Mineralogy and Petrology*, **139**, 163 – 179.

Barker, A.J. (1995): Post-entrapment modification of fluid inclusions due to overpressure: evidence from natural samples. *Journal of Metamorphic Geology*, **13**, 737-750.

Berman, R. G., (1988): Internally-consistent thermodynamic data for minerals in the system Na_2O - K_2O - CaO - MgO - FeO - Fe_2O_3 - Al_2O_3 - SiO_2 - TiO_2 - H_2O - CO_2: Journal of Petrology, **29**, 445-522.

Bodnar, R.J., Binns, P.R., & Hall, D.L. (1989): Synthetic fluid inclusions-VI. Quantitative evaluation of the decrepitation behavior of fluid inclusions in quartz at one atmosphere confining pressure. *Journal of Metamorphic Geology*, **7**, 229-242.

Brown, P.E. (1989): FLINCOR: A microcomputer program for the reduction and investigation of fluid inclusion data. *American Mineralogist*, **74**, 1390-1393.

Brown, P.E. & Lamb, W.M. (1989): P-V-T properties of fluids in the system $H_2O \pm CO_2 \pm NaCl$: New graphical presentations and implications for fluid inclusion studies. *Geochimica et Cosmochimica Acta*, **53**, 1209-1221.

Cordier, P., Doukhan, J.C., & Ramboz, C. (1994): Influence of dislocations on water leakage from fluid inclusions in quartz: a quantitative reappraisal. *European Journal of Mineralogy*, **6**, 745 – 752.

El-Shazly, A.K. (1994): Petrology of lawsonite, pumpellyite and sodic amphibole - bearing rocks from Saih Hatat, NE Oman. *Journal of Metamorphic Geology*, 12, 23-48.

El-Shazly, A.K. (1995): Petrology of Fe-Mg carpholite-bearing metasediments from NE Oman. *Journal of Metamorphic Geology*, **13**, 379-396.

El-Shazly, A.K. (1996): Petrology of Fe-Mg carpholite-bearing metasediments from NE Oman: Reply to comments by Vidal and Theye. *Journal of Metamorphic Geology*, **14**, 386-397.

El-Shazly, A.K. (2001): Are pressures for blueschists and eclogites overestimated? The case from NE Oman. *Lithos*, **56**, 231-264.

El-Shazly, A.K. & Coleman, R.G. (1990): Metamorphism in the Oman Mountains in relation to the ophiolite emplacement. *in* "The Geology and Tectonics of the Oman Region" Robertson, A. H. F., Searle, M. P. and Ries, A., eds, *Geological Society, London, Special Publication*, **49**, 475-495.

El-Shazly, A.K. & Sisson, V.B. (1999): Retrograde evolution of eclogites and blueschists from NE Oman: Evidence from fluid inclusions and petrological data. *Chemical Geology*, **154**, 193-223.

El-Shazly, A. K.; Coleman, R. G. & Liou, J. G. (1990): Eclogites and blueschists from NE Oman: Petrology and P-T evolution: Journal of Petrology, **31**, 629-666.

El-Shazly, A.K., Bröcker, M., Hacker, B. & Calvert, A. (2001): Formation and exhumation of blueschists and eclogites from NE Oman: new perspectives from Rb-Sr and $^{40}Ar/^{39}Ar$ dating. *Journal of Metamorphic Geology*, **19**, 233-248

Gao, J. & Klemd, R., (2001): Primary fluids entrapped at blueschist to eclogite transition: evidence from the Tianshan meta-subduction complex in northwestern China. *Contrib. Mineral. Petrol.,* **142**, 1-14.

Glennie, K.W., Boeuf, M.G.A., Hughes Clark, M.H.W., Moody-Stuart, M, Pilaar, W.F. and Reinhardt, B.M. (1974): Geology of the Oman mountains, Verhandelingen van het Koninklijk Nederlands Geologischs Mijnbouwkundig Genootschap, **31,** 1-423.

Goffé, B., Michard, A.; Kienast, J.R. & Le Mer, O. (1988): A case of obduction related high P low T metamorphism in upper crustal nappes, Arabian continental margin, Oman: P-T paths and kinematic interpretation: *Tectonophysics*, **151**, 363-386.

Goldstein, R.H., & Reynolds, T.J. (1994): Systematics of fluid inclusions in diagenetic minerals. *SEPM short course*, **31**, 199 pp.

Gregory, R.T., Gray, D.R., & Miller, J. McL. (1998): Tectonics of the Arabian margin associated with the formation and exhumation of high pressure rocks, Sultanate of Oman. *Tectonics*, **17**, 657-670.

Hall, D.L. Sterner, M.S. (1993): Preferential water loss from synthetic fluid inclusions. *Contrib. Mineral. Petrol.,* **114**, 489-500.

Hurai, V., Janák, M., Ludhová, L., Horn, E.E., Thomas, R., Majzlan, J. (2000): Nitrogen-bearing fluids, brines and carbonate liquids in Variscan migmatites of the Tatra Mountains, Western Carpathians - heritage of high-pressure metamorphism. *Eur. J. Mineral.*, 12, 1283 – 1300.

Klemd, R., van den Kerkhof, A. M., and Horn, E. E. (1992): High-density CO_2 - N_2 inclusions in eclogite facies metasediments of the Münchberg gneiss complex, SE Germany. *Contributions to Mineralogy and Petrology*. **111**, 409 - 419.

Küster, M. & Stöckhert, B. (1997): Density changes of fluid inclusions in high-pressure low-temperature metamorphic rocks from Crete: A thermobarometric approach based on the creep strength of the host minerals. *Lithos,* **41**, 151-167.

Le Métour, J.; de Gramont, X.; Villey, M. (1986): Geological map of Masqat and Quryat, sheets NF40-4A, NF40-4D and explanatory notes. Scale 1:100,000. Ministry of Petroleum and Minerals, Directorate General of Minerals, Sultanate of Oman.

Le Métour, J., Rabu, D., Tegyey, M., Bechennec, F.; Beurrier, M. & Villey, M. (1990). Subduction and obduction: two stages in the Eo-Alpine tectonometamorphic evolution of the Oman Mountains. *in* "The Geology and Tectonics of the Oman Region". Robertson, A. H. F., Searle, M. P. and Ries, A. C. (eds), *Geological Society, London, Special Publication*, **49**, 327-339.

Miller, J. M. L., Gray, D. R., & Gregory, R. T. (1998): Exhumation of high pressure rocks in northeastern Oman. *Geology*, **26**, 235-238.

Perkins, E. H., Brown, T. H. & Berman, R. G. (1986): PTX-system: three programs for calculation of P-T composition phase diagrams. *Computers and Geosciences*, **12**: 749-755.

Ramsay, J.G. & Huber, M.I. (1983): The Techniques of Modern Structural Geology, 1, *Academic press*, 307p.

Roedder, E. (1984): Fluid Inclusions. *Reviews in Mineralogy*, 12, 644 pp.

Robertson, A. H. F. (1987): Upper Cretaceous Muti Formation: transition of a Mesozoic nate platform to a foreland basin in the Oman Mountains. *Sedimentology*, **34**, 1123-1142.

Scambelluri, M. (1992): Retrograde fluid inclusions in eclogitic metagabbros from the Ligurian Western Alps. *European Journal of Mineralogy*, **4**, 1097 - 1112.

Scambelluri, M., Pennacchioni, G., & Philippot, P. (1998): Salt – rich aqueous fluids formed during eclogitization of metabasites in the Alpine continental crust (Austroalpine Mt. Emilius unit, Italian western Alps). *Lithos*, **43**, 151 – 167.

Searle, M. P., Waters, D. J., Martin, H. N. & Rex, D. C. (1994): Structure and metamorphism of blueschist-eclogite facies rocks from the northeastern Oman Mountains. *Journal of the Geological Society, London*, **151**, 555-576.

Sterner, S.M., & Bodnar, R.J. (1989): Synthetic fluid inclusions - VII. Re-equilibration of fluid inclusions in quartz during laboratory-simulated metamorphic burial and uplift. *Journal of Metamorphic Geology*, **7**: 243-260.

Sterner, S.M., Hall, D.L., & Keppler, H. (1995): Compositional re-equilibration of fluid inclusions in quartz. *Contrib. Minera.l Petrol.,***119**, 1-15.

Touret, J. L. R. (1992): Fluid inclusions in subducted rocks. *Proceedings Koninklijke Nederlandse Akademie van Wetenschappen*, **95** (3), 385 - 403.

Vallis, F. & Scambelluri, M. (1996). Redistribution of high pressure fluids during retrograde metamorphism of eclogite-facies rocks (Voltri Massif, Italian Western Alps). *Lithos*, **39**, 81 – 92.

Van den Kerkhof, A.M. & Hein, U.F. (2001). Fluid inclusion petrography. *Lithos*, **55**, 27 –47.

Vidal, O., Goffé, B. & Theye, T. (1992): Experimental study of the stability of sudoite and magnesiocarpholite and calculation of a new petrogenetic grid for the system FeO-MgO-Al_2O_3-SiO_2-H_2O. *Journal of Metamorphic Geology*, **10**, 603-614.

Vidal, O. & Theye, T. (1996): Petrology of Fe-Mg-carpholite-bearing metasediments from NE Oman; discussion, *Journal of Metamorphic Geology*, **14**,381-386.

Vityk, M.O. & Bodnar, R.J. (1995): Textural evolution of synthetic fluid inclusions in quartz during reequilibration, with applications to tectonic reconstruction. *Contributions to Mineralogy and Petrology*, **119**, 309-323.

Vityk, M.O. & Bodnar, R.J. (1995a): Do fluid inclusions in high-grade metamorphic terranes preserve peak metamorphic density during retrograde decompression? *American Mineralogist*, **80**, 641-644.

Vityk, M.O., Bodnar, R.J. & Schmidt, C.S. (1994): Fluid inclusions as tectonothermobarometers: Relation between pressure – temperature history and reequilibration morphology during crustal thickening. *Geology*, **22**, 731 – 734.

Vry, J. K., and Brown, P. E. (1991): Texturally-early fluid inclusions in garnets: evidence of the prograde metamorphic path? *Contributions to Mineralogy and Petrology*, **108**, 271 - 282.

Winslow, D. M., Bodnar, R. J., and Tracy, R. J. (1994): Fluid inclusion evidence for an anticlockwise metamorphic P-T path in central Massachusetts. *Journal of Metamorphic Geology*, **12**, 361 - 371.

Zhang, Y. & Franz, J.D. (1987): Determination of the homogenization temperatures and densities of supercritical fluids in the system NaCl-KCl-$CaCl_2$-H_2O using synthetic fluid inclusions. *Chemical Geology*, **64**, 335-350.

Figure Captions

Figure 1: Geological map of Saih Hatat, NE Oman, simplified after Le Métour *et al.* (1986) and Gregory *et al.* (1998), and showing the locations of the samples studied. Regions I, II and III and metamorphic zones A, B and C are from El-Shazly & Coleman (1990). Right hand key: allochthonous units, left hand one: autochthonous units. Q: Quaternary, T: Tertiary; K: Cretaceous, Tr: Triassic, J: Jurassic, P: Permian, p€: Precambrian.

Figure 2: (a & b) Tubular inclusions in carpholite (type A_{Car}), sample R-97. (a) Inclusion is 20 μm long; and (b) 12 μm long. (c) Isolated inclusion in Qz (Type A_{Qz}), R-97. Inclusion size is 5 μm. (d) Type C_{Car} inclusions crossing Car and Qz crystals, R-97. Note type A_{Car} inclusions in lower left quarter (shown by arrow). Scale bar = 10 μm. (e) CO_2 – bearing inclusion in Qz (type X_{Qz}) with a low shape factor, III-90. Scale bar = 30 μm.

Figure 3: Histograms of Tm_f values for upper plate samples.

Figure 4: Histograms of T_h values for upper plate samples.

Figure 5: Plots of (a) T_h vs. Volume equivalent spherical radius (VESR), (b) shape factor, and (c) Tm_f for R-97.

Figure 6: Plots of (a) T_h vs. Volume equivalent spherical radius (VESR), (b) shape factor, and (c) Tm_f for Mj-14.

Figure 7: Plots of (a) T_h vs. Volume equivalent spherical radius (VESR), (b) shape factor, and (c) Tm_f for Am-4. Open symbols (type A') represent inclusions of type A with lower degrees of fill.

Figure 8: Histograms of Tm_f and T_h values for lower plate samples.

Figure 9: Plot of Tm_f vs. T_h. for the lower plate samples.

Figure 10: Equilibrium curves used to constrain the P-T conditions of metamorphism of Upper plate samples (cf. El-Shazly, 1996); (1) 2 Mcar = Sud + Qz, (1b) and (1c) are isopleths for reaction (1) calculated at a_{Mcar} = 0.85 and 0.65, representing Car compositions in samples Sq-1 (Permian units) and Am-4, respectively; (2) 5 Mcar + 9 Qz = Chl + 4 Prl + 2 H_2O; (3) 5 Sud + 23 Qz = 2 Chl + 8 Prl + 4 H_2O; (4) Fcar = Fctd + Qz + H_2O. Equilibrium curves of the same reaction calculated for a_{Fcar} = 0.76, a_{Fctd} = 0.88 (4a), a_{Fcar} = 0.69, a_{Fctd} = 1(4b), a_{Fcar} = 0.64, and a_{Fctd} = 1 (4c), are also shown as dotted curves, and correspond to mineral compositions in Permian and Jurassic units. (5) 5 Dap + 8 Pg + 6 Qz = 4 Fgln + 13 Fctd + 11 H_2O; (5a) reaction (5) calculated for a_{Dap} = 0.05, a_{Fgln} = 0.1 and a_{Fctd} = 0.75, corresponding to mineral compositions in Am-3, and average composition of chloritoid from Region III. (6) Arag = Cc after Johannes and Puhan (1971). (7) Lower pressure stability limit of lawsonite after Liou (1971). (8) The

reaction Ab = Jd + Qz calculated for a_{Jd} = 0.27. (9) Kln + 2 Qz = Prl + H_2O. (10) Prl = And + 3 Qz + H_2O. (11) Prl = Ky + 3 Qz + H_2O. P-T conditions of metamorphism of the Cretaceous (R-97), Permian (Mj-14) and Proterozoic (Am-4) samples are represented by the dark and light stipple, respectively. Isochores for type A_{Qz} are shown as thick dashed lines, for type B_{Qz} as thin dashed lines, and for type A_{Car} as a solid line, each labeled with sample number.

Fig. 11: P-T conditions of metamorphism of zone A (light stipple) constrained by the intersection of the equilibria: (1) Jd + Qz = Ab; (1), (1b) and (1c) are isopleths of the same reaction for X_{Jd} = 0.27 and 0.18, respectively, (2) Lw + Ab = Czo + Pg + Qz + H_2O; (3) Ab + Cc + Chl + Qz = Gln + Czo + H_2O + CO_2 (4) Ab + Chl + Tr = Gln + Czo + Qz + H_2O; both activity corrected for III-80 and XCO_2 = 0.05; (5) Dap + Pg + Qz = Fgln + Fctd + H_2O calculated for a_{dap} = 0.05, a_{fgln} = 0.1; a_{fctd} = 0.75; (6) Rt + Cc + Qz = Ttn + CO_2 calculated with X_{CO2} = 0.05; (7) isochore for a type B_{Qz} inclusion, III-181 (dash-dotted line); (8) isochore for a CO_2 bearing inclusion, III-90 (long dashes). Unless otherwise indicated, all reactions for Figs. 13 & 14 were calculated using GE0-CALC (Perkins et al., 1986), the data base of Berman (1988), and the data of El-Shazly (1994, 1995) for Gln, Fgln, Fctd, and Dap.

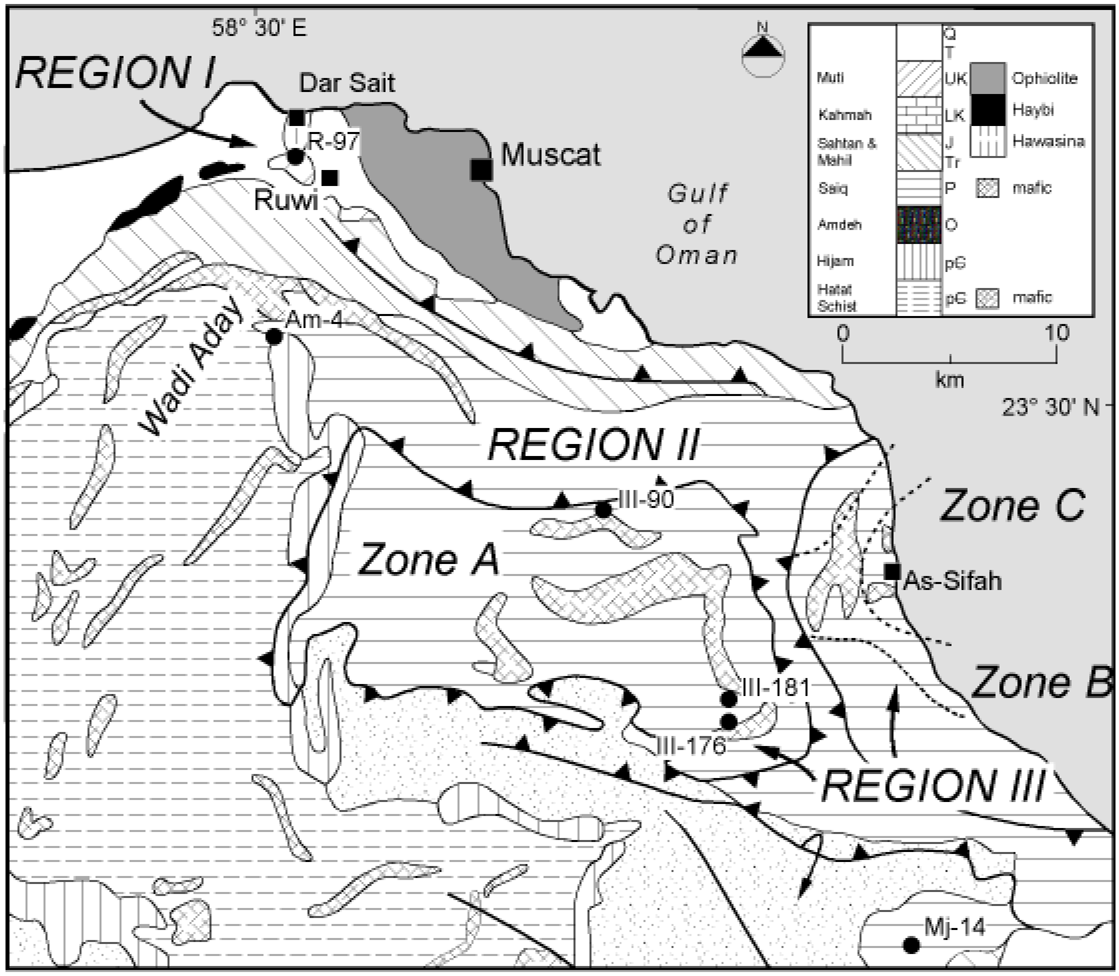
58° 30' E
REGION I
Dar Sait
R-97
Ruwi
Muscat
Gulf of Oman
Am-4
Wadi Aday
REGION II
III-90
Zone A
Zone C
As-Sifah
Zone B
III-181
III-176
REGION III
Mj-14
23° 30' N
N
Muti
Kahmah
Sahtan & Mahil
Saiq
Amdeh
Hijam
Hatat Schist
Q T
UK
LK
J Tr
P
O
pG
pG
Ophiolite
Haybi
Hawasina
mafic
mafic
0
10
km

Fig. 1

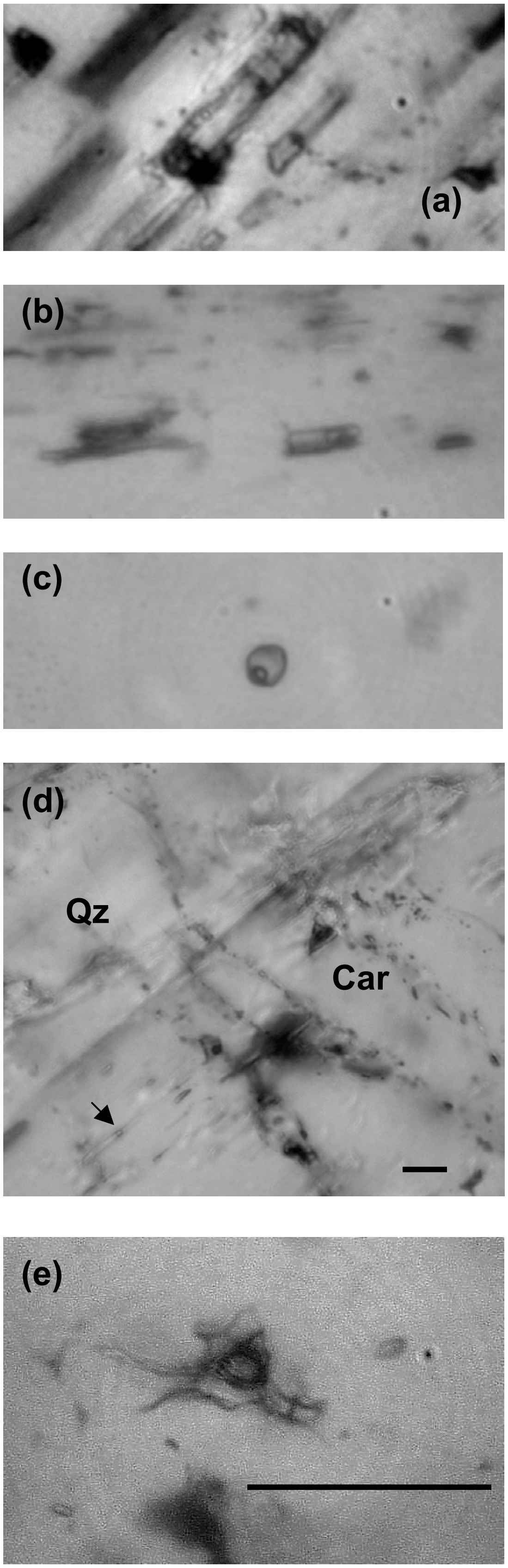

Fig. 2

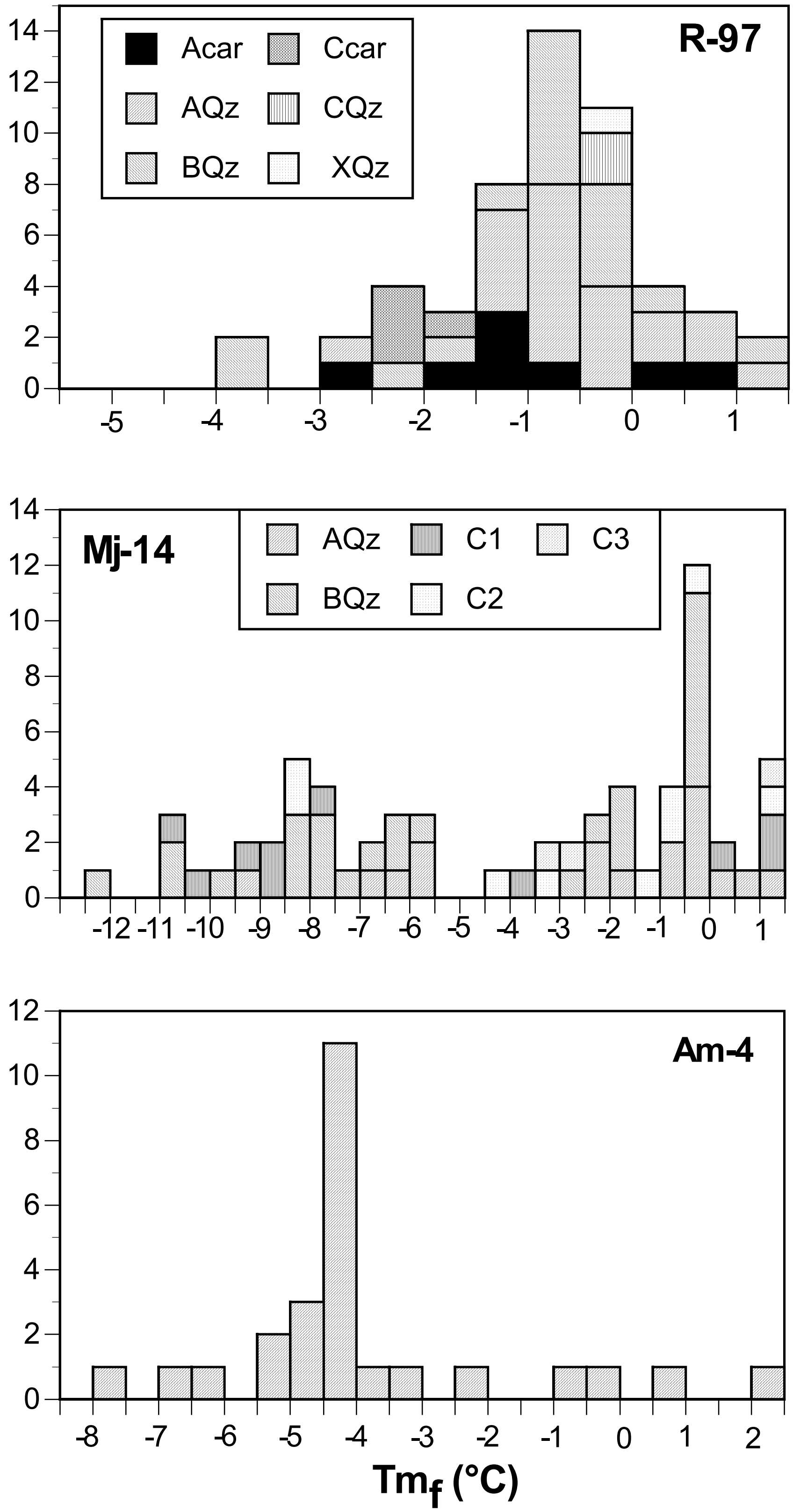

Fig. 3

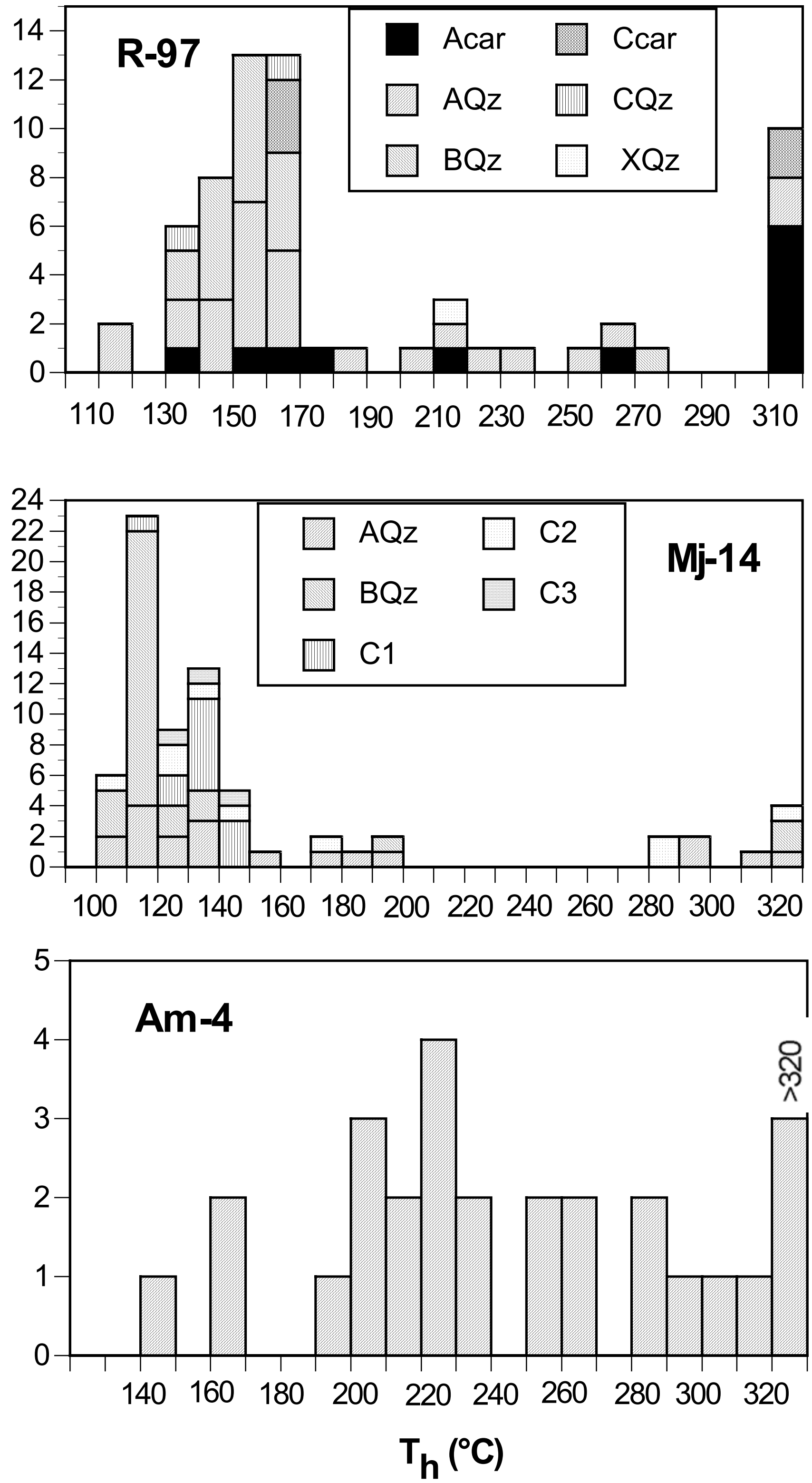

R-97
Acar
Ccar
AQz
CQz
BQz
XQz
14
12
10
8
6
4
2
0
110
130
150
170
190
210
230
250
270
290
310
Mj-14
AQz
C2
BQz
C3
C1
24
22
20
18
16
14
12
10
8
6
4
2
0
100
120
140
160
180
200
220
240
260
280
300
320
Am-4
5
4
3
2
1
0
>320
140
160
180
200
220
240
260
280
300
320
T_h (°C)

Fig. 4

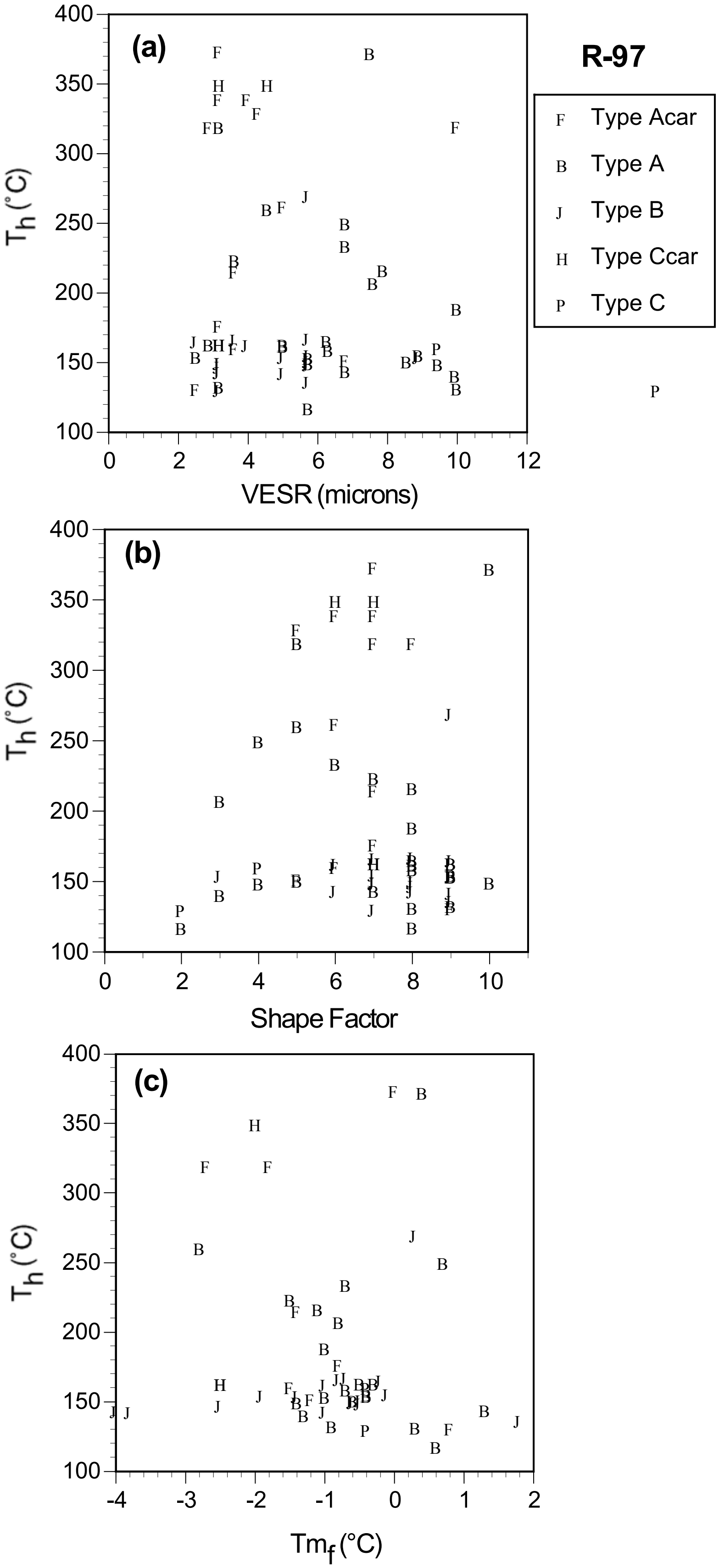
R-97
(a)
(b)
(c)
F Type Acar
B Type A
J Type B
H Type Ccar
P Type C
Th (°C)
VESR (microns)
Shape Factor
Tmf (°C)

Fig. 5

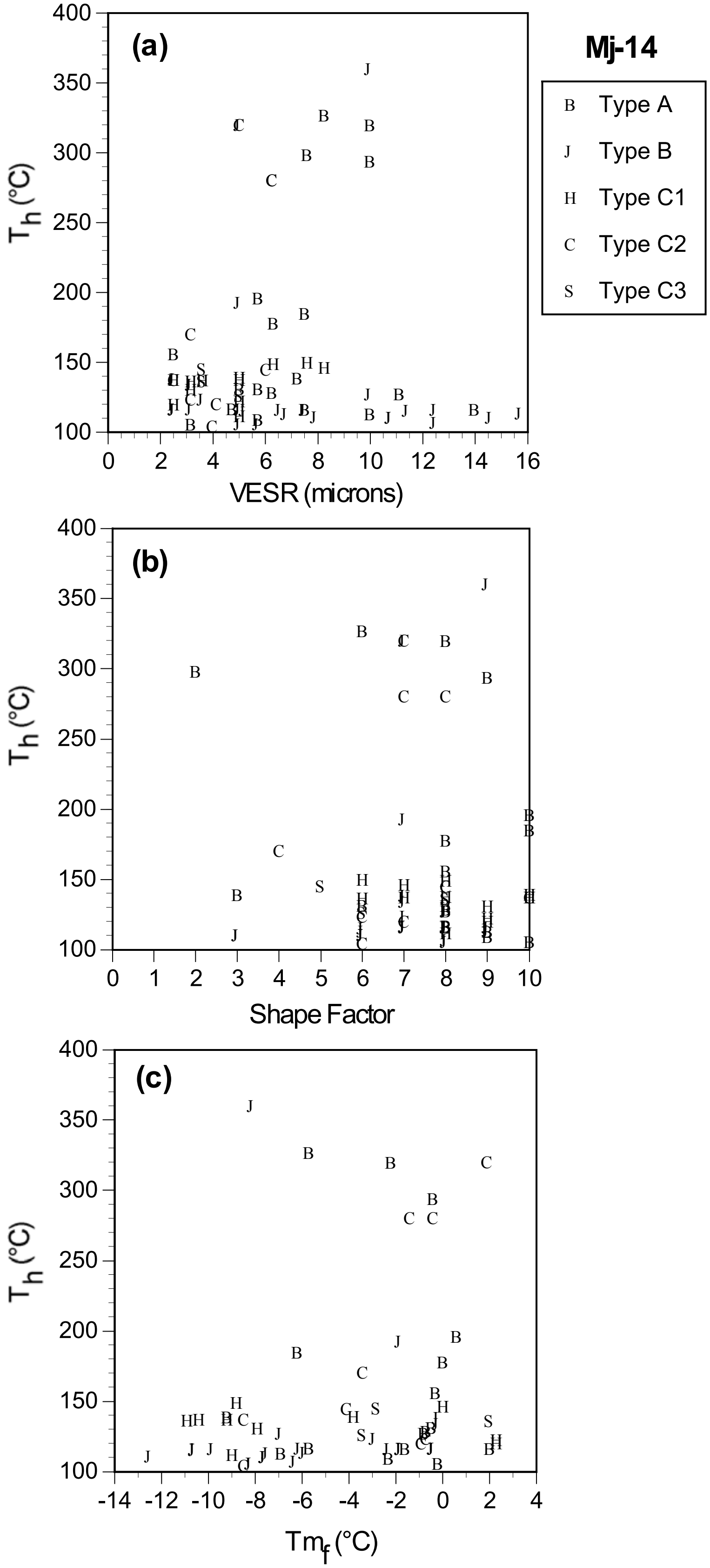
Mj-14
B Type A
J Type B
H Type C1
C Type C2
S Type C3
(a)
Th (°C)
VESR (microns)
(b)
Th (°C)
Shape Factor
(c)
Th (°C)
Tmf (°C)

Fig. 6

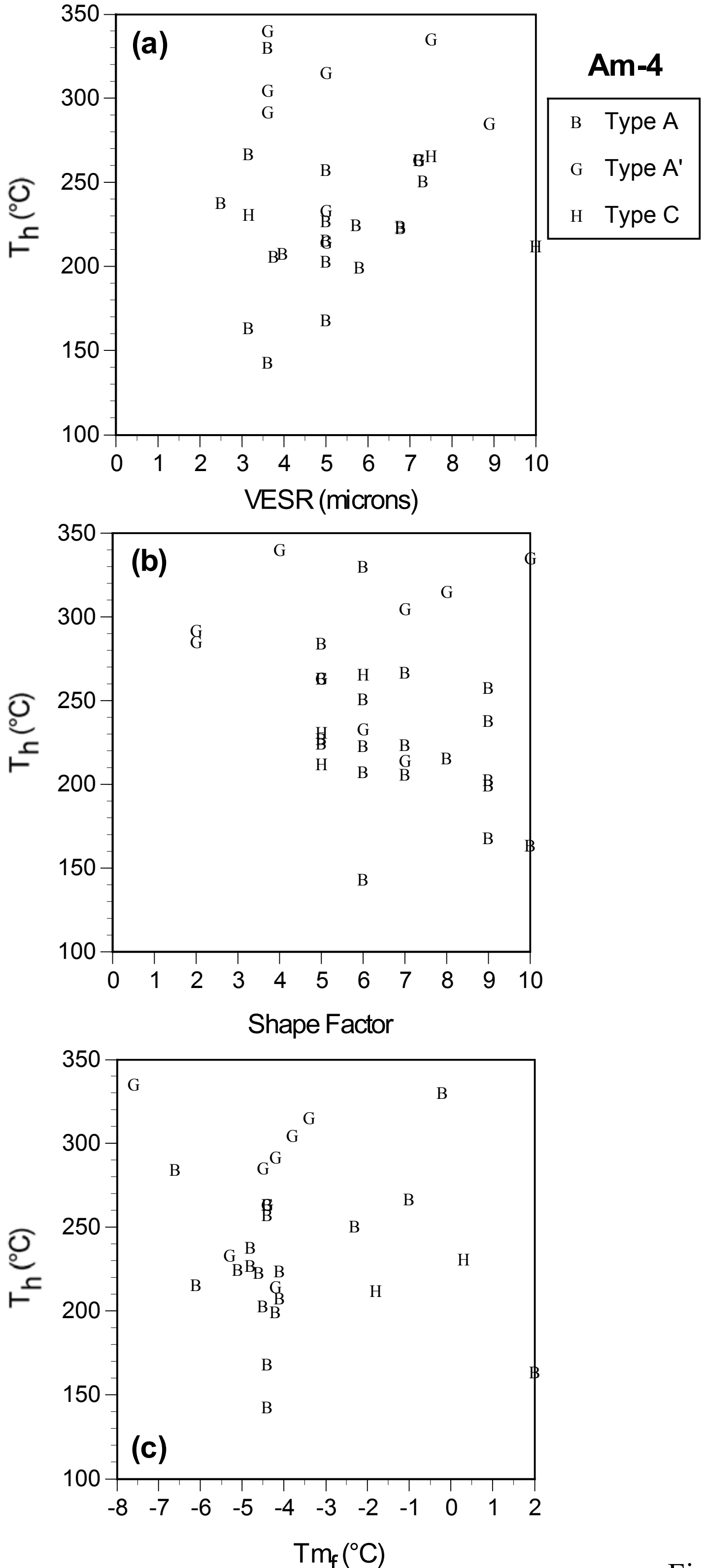

Am-4
Type A
Type A'
Type C
(a)
(b)
(c)
Th (°C)
VESR (microns)
Shape Factor
Tmf (°C)

Fig. 7

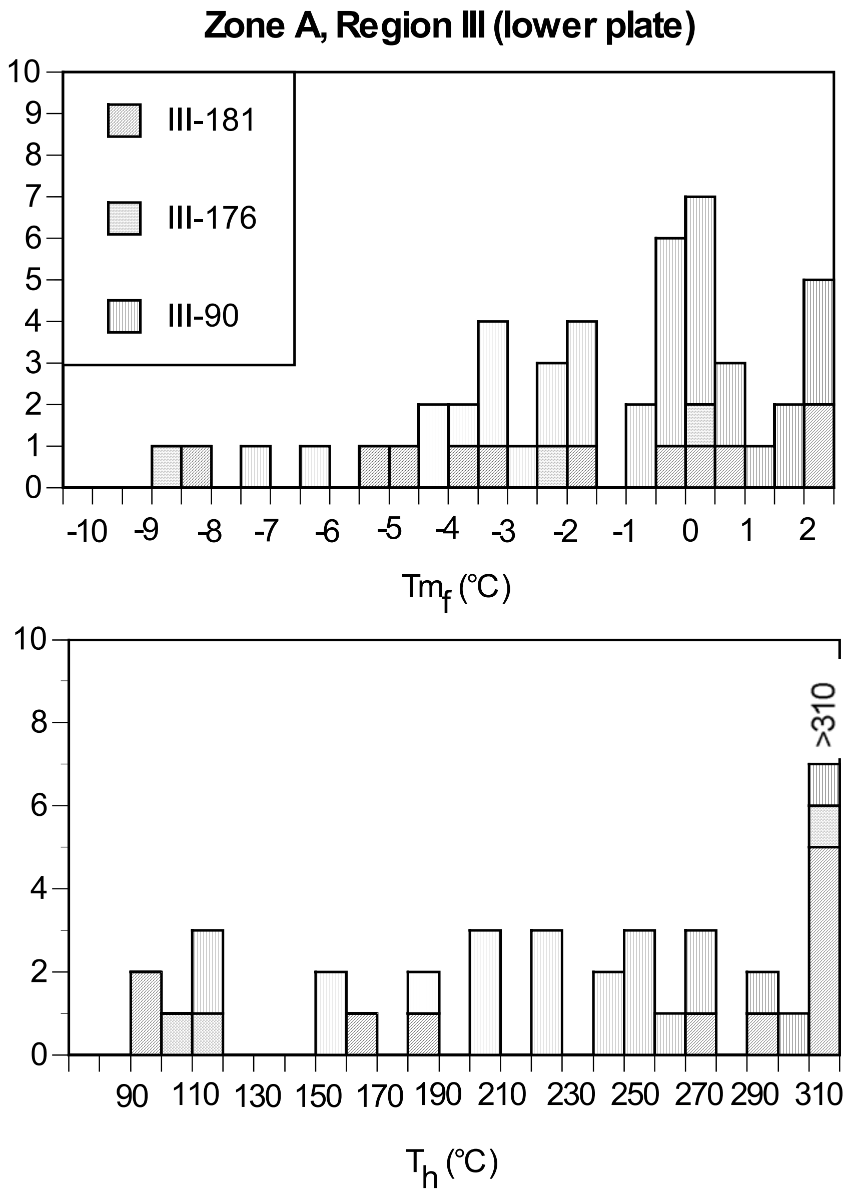
Zone A, Region III (lower plate)
III-181
III-176
III-90
Tmf (°C)
>310
Th (°C)

Fig. 8

Fig. 9

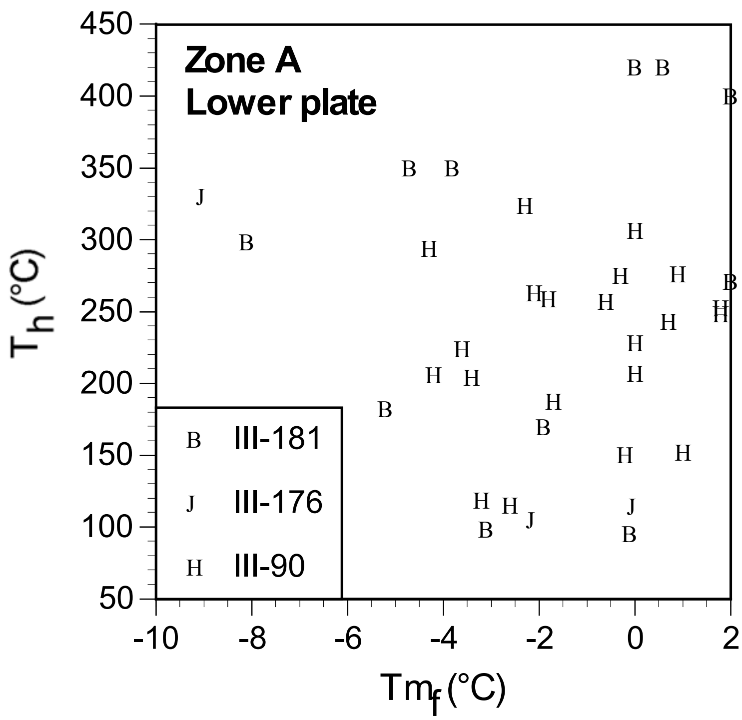
Zone A
Lower plate
B III-181
J III-176
H III-90
T_h (°C)
Tm_f (°C)
450
400
350
300
250
200
150
100
50
-10
-8
-6
-4
-2
0
2

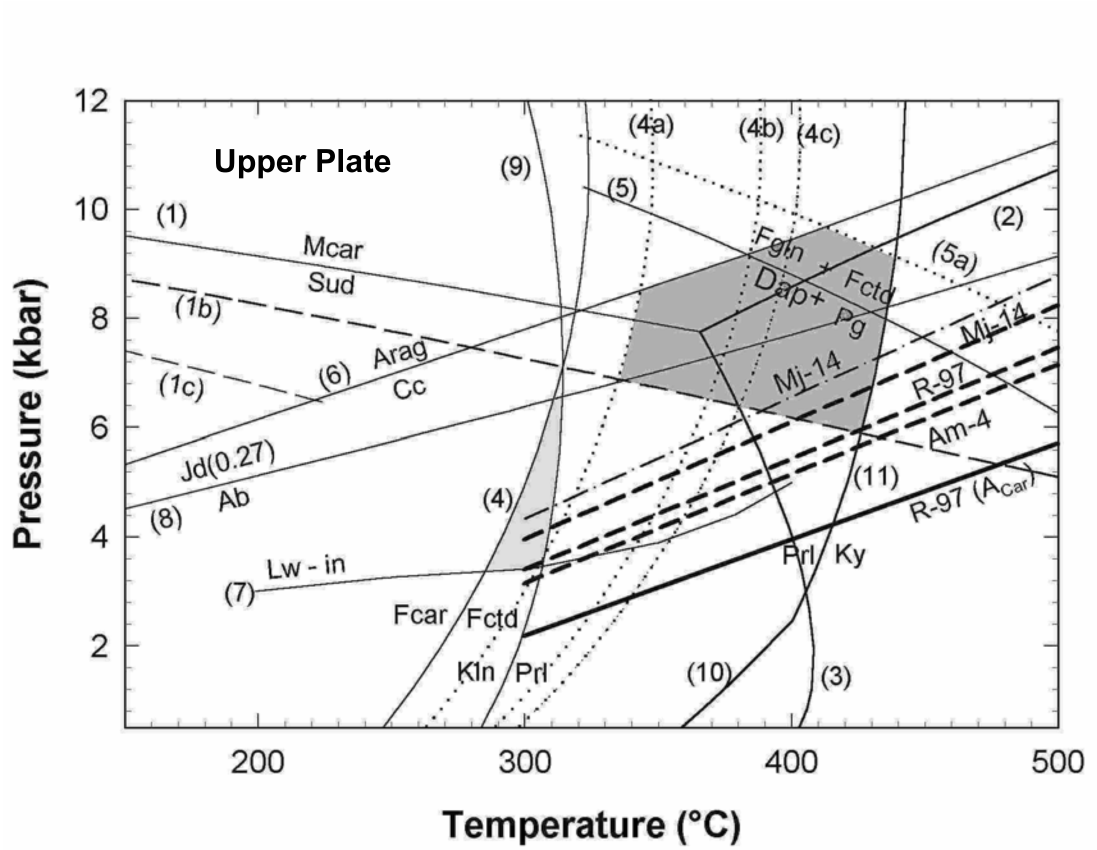

Upper Plate
Pressure (kbar)
Temperature (°C)
12
10
8
6
4
2
200
300
400
500
(1)
(1b)
(1c)
(2)
(3)
(4)
(4a)
(4b)
(4c)
(5)
(5a)
(6)
(7)
(8)
(9)
(10)
(11)
Mcar
Sud
Arag
Cc
Jd(0.27)
Ab
Lw - in
Fcar
Fctd
Kln
Prl
Prl
Ky
Fgln + Fctd
Dap+ Pg
Mj-14
Mj-14
R-97
Am-4
R-97 (ACar)

Fig. 10

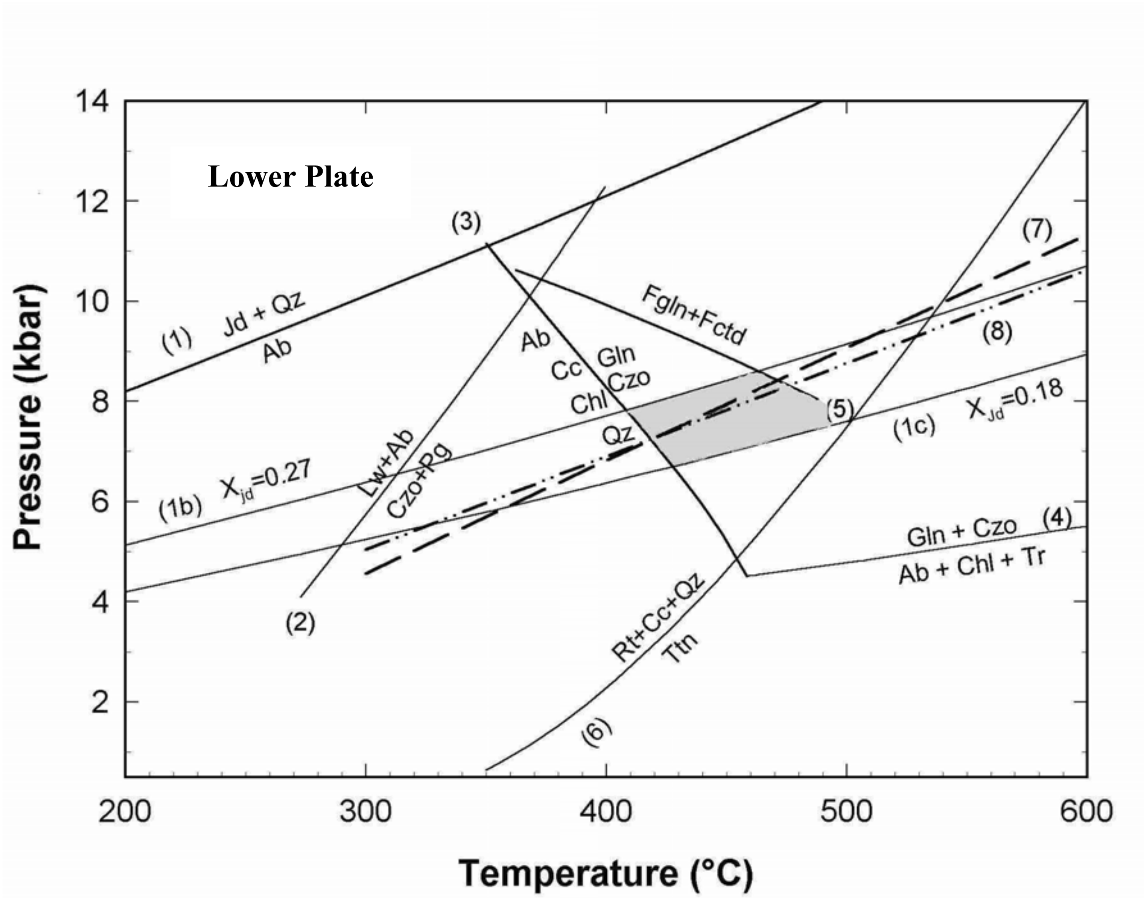
Lower Plate
Pressure (kbar)
Temperature (°C)
(1) Jd + Qz
Ab
(1b) X_{jd}=0.27
(1c) X_{Jd}=0.18
(2) Lw+Ab
Czo+Pg
(3)
Ab
Cc
Chl
Qz
Gln
Czo
Fgln+Fctd
(4) Gln + Czo
Ab + Chl + Tr
(5)
(6) Rt+Cc+Qz
Ttn
(7)
(8)
14
12
10
8
6
4
2
200
300
400
500
600

Fig. 11

Table 1: Petrography of samples studied

Sample #	Region	Locality	Unit	Mineralogy	X_{Fe}	Remarks
R-97*	I	Hamiriya	Muti	Car-Qz-Cc-Chl-Opq-WM	Car: 0.63-0.69 Chl: 0.55-0.57	Vein crosscutting schists with Car-Qz-Cc-Ill-Pg-Rt-Hm-Kln; part of the metamorphosed tectonic melange; Chl forms along rims and fractures of Car.
Mj-14	II	Wadi Mijlas	Saiq	Car-Ctd-Prl-Ph-Pg-Qz-Opq-Tm	Car:0.47-0.71 Ctd:0.89-0.93	Represents a metamorphosed paleosol in the middle of the Saiq formation; Ctd in radiating clusters along rims of Car
Am-4	II	Amarat	Saiq	Car-Qz-Chl-Prl-Cc-Opq-Tm-Rt-Oxychl	Car:0.35-0.41 Chl:0.44-0.5	Deepest unit of the Saiq formation, unconformably overlying Pg - Musc - Chl - Qz schists of the Hatat formation; has two foliations and crosscut by veins; Prl oriented parallel to S2, but not in veins.
III-90	III	E of Wadi Shakry	Saiq	Qz-Ph-Pg-Rt-Opq@Ctd-Chl-Ap-Cc		Prominent S-C fabric, most micas oriented with S2; pressure shadows around Ctd.
III-176	III	S of Wadi Hulw	Saiq	Qz-WM-Chl-Ab-Ep/Czo-Ttn		Unoriented Chl pseudomorphing amphibole? S-C fabric.
III-181	III	S of Wadi Hulw	Saiq	Qz-Ph-Chl-Ep-Ab-Ttn-Ap-Alln		Ep porphyroblasts with cores of Alln; S-C fabric.

*Vein sample; map unit denotes host rock.

Table 2: Summary of microthermometric results for the different fluid inclusion types

Sample (Region)	**FIT**	**Description**	**Tm_e (°C)**		**Tm_f(°C)**		**T_h(°C)**		**Fluid composition**	**Salinity** (wt% NaCl eq.)
			min	max	min	max	min	max		
R-97 (I)	A_{car}	Solitary	-47	-19.8	-2.7	+0.8	131.6	>350	$NaCl-MgCl_2-H_2O$ $NaCl - H_2O$	0 – 4.39
	A_{Qz}/B_{Qz}	Solitary/ cluster	-80	-21	-3.8	+1.8	117.7	>320	$NaCl-MgCl_2-H_2O$ $NaCl - H_2O$?	0 – 6.16
	C_{car}	Healed fractures			-2	-2.5	163.6	>320		3.39 – 4.18?
	C_{Qz}	Healed fractures			-0.4		130	161		0.71?
Mj-14 (II)	A_{Qz}/B_{Qz}	Solitary/ cluster	-51	-19.8	-12.5	+2	107	360	$NaCl-H_2O$ $NaCl-MgCl_2-H_2O$	0 – 16.43
	C_{Qz}	Healed fractures	-52.7	-20.9	-10.9	+2.3	104.4	280.5	$NaCl-CaCl_2-H_2O$ $NaCl-H_2O$	0 - 14.87
Am-4 (II)	A_{Qz}/B_{Qz}	Solitary/ cluster	-50.1	-21.2	-7.6	+2	143	335.1	$NaCl-H_2O$ $NaCl-MgCl_2-H_2O$	0 - 11.22
III-176, III-181 (II)	A_{Qz}/B_{Qz}	Solitary/ cluster	-76	-33.2	-8.5	+2	95	> 400	$NaCl-H_2O$ $NaCl-MgCl_2-H_2O$	0 – 12.28
III-90 (II)	A_{Qz}/B_{Qz}	Solitary/ cluster	-75	-21.5	-4.2	+1.8	115	323.8	$NaCl-MgCl_2-H_2O$	0 – 6.74
	X_{Qz}	3-phase	-39.1	-21.2	-7.1	+3			$NaCl-H_2O-CO_2$	0 – 10.49